
The Representation Jensen-Shannon Divergence

Jhoan K. Hoyos-Osorio
ECE department
University of Kentucky
Lexington, KY
keider.hoyos@uky.edu

Luis G. Sanchez-Giraldo
ECE department
University of Kentucky
Lexington, KY
luis.sanchez@uky.edu

Abstract

Statistical divergences quantify the difference between probability distributions finding multiple uses in machine-learning. However, a fundamental challenge is to estimate divergence from empirical samples since the underlying distributions of the data are usually unknown. In this work, we propose the representation Jensen-Shannon Divergence, a novel divergence based on covariance operators in reproducing kernel Hilbert spaces (RKHS). Our approach embeds the data distributions in an RKHS and exploits the spectrum of the covariance operators of the representations. We provide an estimator from empirical covariance matrices by explicitly mapping the data to an RKHS using Fourier features. This estimator is flexible, scalable, differentiable, and suitable for minibatch-based optimization problems. Additionally, we provide an estimator based on kernel matrices without having an explicit mapping to the RKHS. We show that this quantity is a lower bound on the Jensen-Shannon divergence, and we propose a variational approach to estimate it. We applied our divergence to two-sample testing outperforming related state-of-the-art techniques in several datasets. We used the representation Jensen-Shannon divergence as a cost function to train generative adversarial networks which intrinsically avoids mode collapse and encourages diversity.

1 Introduction

Divergences quantify the difference between probability distributions. In machine learning, divergences can be applied to a wide range of tasks including generative modeling (Generative adversarial networks, variational auto-encoders), two-sample testing, anomaly detection, and distribution shift detection. A fundamental challenge to using divergences in practice is that the underlying distribution of data is unknown and thus divergences must be estimated from observations. Several divergence estimators have been proposed [1–13]. Most of them fall into 4 categories: plug-in, kernel density estimation, k -nearest neighbors, and neural estimators.

Modern machine-learning applications demand estimators that are scalable (capable of managing or processing a vast quantity of data samples), differentiable (suitable for back-propagation), and compatible with minibatch-based optimization [14, 13]. In alignment with this view, we propose a novel divergence based on covariance operators in reproducing kernel Hilbert spaces (RKHS). Our approach embeds the data distributions in an RKHS and exploits the spectrum of the covariance operators of the representations. This quantity resembles the quantum Jensen-Shannon divergence, however, the interpretation and the role of the operators differ.

More concretely, the contributions of this work are the following: 1. We introduce the representation Jensen-Shannon (JS) divergence, as well as a non-parametric estimator from samples which avoids explicit estimation of the underlying distributions of data. 2. We propose an adaptable RKHS based on Fourier features that can be adjusted to maximize the divergence between distributions. This estimator is scalable, differentiable, and suitable for minibatch-based optimization problems. 3. We

show that the representation Jensen-Shannon divergence is a lower bound on the true Jensen-Shannon divergence, which naturally yields a variational estimator of the true Jensen-Shannon divergence. 4. For training generative networks, we empirically show that our divergence prevents mode collapse, leading to more accurate and diverse results. 5. When applied to two-sample testing, the representation Jensen-Shannon divergence outperforms related state-of-the-art techniques.

1.1 Related work

The family of F-divergences, and Integral probability metrics (IPMs)[15] are popular statistical divergences to measure the dissimilarity between probability distributions. F-divergences include the well-known Kullback Leibler (KL) [16, 14] and Jensen-Shannon (JS) divergences [17, 18]. Examples of IPMs include Maximum Mean Discrepancy (MMD) [19, 20] and Wasserstein distances [21, 22]. F-divergences and some IPMs can be formulated as a variational problem:

$$D_{\mathcal{F},\phi}(\mathbb{P}, \mathbb{Q}) = \sup_{f \in \mathcal{F}} \mathbb{E}_{\mathbb{P}} [f(x)] + \mathbb{E}_{\mathbb{Q}} [h \circ f(x)], \quad (1)$$

where h is called a measuring function and \circ denotes function composition [23, 13]. A neural network can be used to define the parameterized function class of *discriminators* \mathcal{F} . This approach is usually referred to as neural estimation [13].

Several machine learning algorithms involving divergences are based on (1) [24–28, 13]. Notwithstanding, the majority of these estimators lack regularization of the complexity and smoothness of the discriminator, resulting in substantial variance and instability during training [14]. The discriminator function space crucially affects the performance of several algorithms involving divergences [29]. For example, in Generative Adversarial Networks (GANs), well-known problems such as lack of diversity and mode collapse result from the generator learning to fool the discriminator by only generating a few realistic samples [30]. To overcome these issues, one can for instance require that the discriminator lies in Reproducing Kernel Hilbert Space (RKHS), which reduces the variance and stabilizes training [14].

The maximum mean discrepancy (MMD) [19] is a divergence computed as the distance between the mean embeddings of the two probability distributions in an RKHS. It can be estimated from finite samples, with $\mathcal{O}(\frac{1}{\sqrt{N}})$ convergence rates, where N is the number of instances. However, due to the underlying geometry, it lacks a straightforward connection with classical information theory tools [31].

Recently, [32] proposed a novel divergence measure that depends on a kernel-based entropy functional, which uses the covariance operators in RKHS implicitly defined by infinitely divisible kernels [33]. This divergence called representation Jensen-Rényi divergence is defined as the matrix-based α -Rényi mutual information between data samples and their labels. Without imposing additional constraints, this divergence can be trivially maximized, and its estimator, which relies on the eigendecomposition of Gram matrices does not scale well.

2 Background

2.1 Classical and quantum Jensen-Shannon divergence

Let \mathbb{P} and \mathbb{Q} be two probability measures defined on a measurable space $(\mathcal{X}, \mathcal{B}_{\mathcal{X}})$, the Jensen-Shannon Divergence (JS) is a measure of statistical distance between \mathbb{P} and \mathbb{Q} and it is defined as:

$$D_{JS}(\mathbb{P}, \mathbb{Q}) = H\left(\frac{\mathbb{P} + \mathbb{Q}}{2}\right) - \frac{1}{2}(H(\mathbb{P}) + H(\mathbb{Q})), \quad (2)$$

where $\frac{\mathbb{P} + \mathbb{Q}}{2}$ represents the mixture of both distributions and $H(\cdot)$ is Shannon’s entropy. Properties of the JS divergence such as boundedness, convexity, symmetry, and its square root being a metric have been extensively studied [34, 35].

Classical probability tools have been used to characterize quantum states represented by *density matrices* which are positive semi-definite, Hermitian, and unit-trace operators acting on a Hilbert space [36]. The eigenvalues of the density matrix are greater or equal to zero, and sum to one, much like a probability mass function. Information theoretic quantities such as entropy or divergence can thus be applied in this context. For example, the *von Neumann* entropy is defined as $S(\rho) = -\text{Tr}(\rho \log \rho) =$

$-\sum_i \lambda_i \log \lambda_i$, where $\{\lambda_i\}$ are the eigenvalues of the density matrix ρ . Quantum divergences measure the distance between quantum states described by two density matrices ρ and σ . The *Quantum Jensen-Shannon divergence* (QJS) is defined as $D_{JS}(\rho, \sigma) = S\left(\frac{\rho+\sigma}{2}\right) - \frac{1}{2}(S(\rho) + S(\sigma))$. QJS divergence is everywhere defined, bounded, symmetric, and zero only if $\rho = \sigma$ [35].

2.2 Mean embeddings and Covariance operators

Let $\{\mathcal{X}, \mathbf{B}_{\mathcal{X}}\}$ be a measurable space and $\kappa : \mathcal{X} \times \mathcal{X} \rightarrow \mathbb{R}_{\geq 0}$ be a positive definite kernel. There exists a mapping $\phi : \mathcal{X} \rightarrow \mathcal{H}$, where \mathcal{H} is a reproducing kernel Hilbert space (RKHS), such that $\kappa(x, x') = \langle \phi(x), \phi(x') \rangle_{\mathcal{H}}$, and $\kappa(x, x) = 1$ for all $x \in \mathcal{X}$. The Kernel mean embedding [37] is a mapping μ from $\mathcal{M}_+^1(\mathcal{X})$, the space of probability measures on \mathcal{X} , to \mathcal{H} defined as follows:

$$\mu_{\mathbb{P}} = \mathbb{E}_{X \sim \mathbb{P}}[\phi(X)] = \int_{\mathcal{X}} \phi(x) d\mathbb{P}(x), \quad \text{for } \mathbb{P} \in \mathcal{M}_+^1. \quad (3)$$

An important property of the mean embedding is that if $\mathbb{E}_{X \sim \mathbb{P}}[\kappa(X, X)] < \infty$, for any $f \in \mathcal{H}$, $\mathbb{E}_{X \sim \mathbb{P}}[f(X)] = \langle f, \mu_{\mathbb{P}} \rangle_{\mathcal{H}}$. Another related mapping is the uncentered covariance operator. In this case, $\mathbb{P} \in \mathcal{M}_+^1$ is mapped to an operator $C_{\mathbb{P}} : \mathcal{H} \rightarrow \mathcal{H}$ given by:

$$C_{\mathbb{P}} = \mathbb{E}_{X \sim \mathbb{P}}[\phi(X) \otimes \phi(X)] = \int_{\mathcal{X}} \phi(x) \otimes \phi(x) d\mathbb{P}(x), \quad (4)$$

Similarly, for any $f, g \in \mathcal{H}$, $\mathbb{E}_{X \sim \mathbb{P}}[f(X)g(X)] = \langle g, C_{\mathbb{P}}f \rangle_{\mathcal{H}}$. For a bounded kernel, the covariance operator is positive semi-definite, Hermitian (self-adjoint), and trace class [33, 31]. The spectrum of the covariance is discrete and consists of non-negative eigenvalues λ_i with $\sum \lambda_i < \infty$.

2.3 Kernel-based information theory

For normalized covariance operators with unit trace, we can define information theoretic quantities on their spectrum (See section 2.1). This was observed in [33] where the kernel-based entropy functional: $S_{\alpha}(C_{\mathbb{P}}) = \frac{1}{1-\alpha} \log [\text{Tr}(C_{\mathbb{P}}^{\alpha})]$, was proposed. $\text{Tr}(\cdot)$ denotes the trace operator and $\alpha > 0$ is the entropy order. This quantity closely resembles *quantum Rényi entropy* [38]. In the limit when $\alpha \rightarrow 1$, $S_{\alpha \rightarrow 1}(C_{\mathbb{P}}) = \text{Tr}(C_{\mathbb{P}} \log C_{\mathbb{P}})$, becomes *Von Neumann entropy*. This connection between covariance operators in RKHSs and information theory has been also discussed in [31].

Let $\mathbf{X} = \{x_i\}_{i=1}^N$ be a set of samples $x \in \mathcal{X}$ following an unknown distribution \mathbb{P} defined on \mathcal{X} . Then, the kernel-based entropy estimator relies on the spectrum of the empirical uncentered covariance operator, which is defined as $\mathbf{C}_X = \frac{1}{N} \sum_i \phi(x_i) \otimes \phi(x_i)$. Similarly, we can construct the Gram matrix \mathbf{K}_X , consisting of all normalized pairwise kernel evaluations of the samples in \mathbf{X} , that is $(\mathbf{K})_{ij} = \kappa(x_i, x_j)$. If we normalize the matrix \mathbf{K}_X such that, $\text{Tr}(\mathbf{K}_X) = 1$, \mathbf{C}_X and \mathbf{K}_X have the same non zero eigenvalues [33]. This yields the kernel-based entropy estimator:

$$S(\mathbf{C}_X) = S(\mathbf{K}_X) = -\text{Tr}(\mathbf{K}_X \log \mathbf{K}_X) = -\sum_{i=1}^n \lambda_i \log \lambda_i, \quad (5)$$

where λ_i represents the i th eigenvalue of \mathbf{K}_X . The matrix-based entropy has been used as a building block for other matrix-based measures such as joint and conditional entropy, mutual information [39], total correlation [40] and divergences [32]. Although this entropy functional bears resemblance with quantum Rényi and von Neumann entropies [41], the role and interpretation of the operators differ.

3 Representation Jensen-Shannon Divergence

Definition 1. Let \mathbb{P} and \mathbb{Q} be two probability measures defined on a measurable space $\{\mathcal{X}, \mathbf{B}_{\mathcal{X}}\}$, and $\phi : \mathcal{X} \rightarrow \mathcal{H}$, be a mapping to a Reproducing Kernel Hilbert space (RKHS) \mathcal{H} , such that $\langle \phi(x), \phi(x) \rangle_{\mathcal{H}} = 1$ for all $x \in \mathcal{X}$. For uncentered covariance operators, $C_{\mathbb{P}}$ and $C_{\mathbb{Q}}$, as defined in (4), the **representation Jensen-Shannon divergence** between $C_{\mathbb{P}}$ and $C_{\mathbb{Q}}$ is defined as:

$$D_{JS}^{\phi}(C_{\mathbb{P}}, C_{\mathbb{Q}}) = S\left(\frac{C_{\mathbb{P}} + C_{\mathbb{Q}}}{2}\right) - \frac{1}{2}(S(C_{\mathbb{P}}) + S(C_{\mathbb{Q}})), \quad (6)$$

Below, we introduce two key properties of the representation JS divergence.

Theorem 1. For all probability measures \mathbb{P} and \mathbb{Q} defined on \mathcal{X} , and covariance operators $C_{\mathbb{P}}$ and $C_{\mathbb{Q}}$ with RKHS mapping $\phi(x)$ such that $\forall x \in \mathcal{X}, \|\phi(x)\| = 1$

$$D_{JS}(C_{\mathbb{P}}, C_{\mathbb{Q}}) \leq D_{JS}(\mathbb{P}, \mathbb{Q}) \quad (7)$$

$$D_{JS}(C_{\mathbb{P}}, C_{\mathbb{Q}}) \geq \frac{1}{8} \|C_{\mathbb{P}} - C_{\mathbb{Q}}\|_*^2 \geq \frac{1}{8} \|C_{\mathbb{P}} - C_{\mathbb{Q}}\|_{HS}^2 \quad (8)$$

Proof: See appendix A.1 in supplementary material.

As a consequence of property (8), we have that for a characteristic kernel κ , the representation JS divergence is non zero if $\mathbb{P} \neq \mathbb{Q}$ since $\|\phi(x) \otimes \phi(x) - \phi(y) \otimes \phi(y)\|_{HS}^2 = \kappa^2(x, x) - 2\kappa^2(x, y) + \kappa^2(y, y)$ and κ^2 is characteristic (see supplementary material for details). As we show below, property (7) can be used to obtain an estimator of JS divergence.

3.1 Estimating the representation Jensen-Shannon divergence

Given two sets of samples $\mathbf{X} = \{x_i\}_{i=1}^N \subset \mathcal{X}$ and $\mathbf{Y} = \{y_i\}_{i=1}^M \subset \mathcal{X}$ with unknown distributions \mathbb{P} and \mathbb{Q} , we propose two estimators of the representation JS divergence.

Covariance-based estimator: Let $\phi_{\omega} : \mathcal{X} \rightarrow \mathcal{H}_D$, be a mapping to a D -dimensional RKHS \mathcal{H}_D , parameterized by ω . We propose to use Fourier features to construct a mapping function to \mathcal{H}_D . Given a shift-invariant kernel $\kappa : \mathcal{X} \times \mathcal{X} \rightarrow \mathbb{R}_{\geq 0}$, the random Fourier Features (RFF) ([42]) is a method to create a *smooth* feature mapping $\phi_{\omega}(x) : \mathcal{X} \rightarrow \mathbb{R}^D$ so that $\kappa(x, x') \approx \langle \phi_{\omega}(x), \phi_{\omega}(x') \rangle$. To generate an RFF mapping, we compute the Fourier transform of the kernel, $p(\omega) = \frac{1}{2\pi} \int e^{-j\omega^\top \delta} \kappa(\delta) d\delta$, which yields probability distribution function from which we draw $D/2$ i.i.d samples $\omega_1, \dots, \omega_{D/2} \in \mathbb{R}^d$. Finally, the mapping is given by $\phi_{\omega}(x) = \sqrt{\frac{2}{D}} [\cos(\omega_1^\top x), \sin(\omega_1^\top x), \dots, \cos(\omega_{D/2}^\top x), \sin(\omega_{D/2}^\top x)]$.

Let $\Phi_X \in \mathbb{R}^{N \times D}$ and $\Phi_Y \in \mathbb{R}^{M \times D}$ be the matrices containing the mapped samples of each distribution. Then, the empirical uncentered covariance matrices are computed as $C_X = \frac{1}{N} \Phi_X^\top \Phi_X$ and $C_Y = \frac{1}{M} \Phi_Y^\top \Phi_Y$. Finally, our divergence estimator is defined as:

$$D_{JS}^{\omega}(\mathbf{X}, \mathbf{Y}) = S(\pi_1 C_X + \pi_2 C_Y) - (\pi_1 S(C_X) + \pi_2 S(C_Y)), \quad (9)$$

where $\pi_1 = \frac{N}{N+M}$ and $\pi_2 = \frac{M}{N+M}$ are the sample proportions of each distribution (e.g. 1/2 if the samples are balanced). We use (5) to estimate the entropies by computing the eigenvalues of the covariance matrices.

Kernel-based estimator Here, we propose an estimator of representation JS divergence from kernel matrices without having an explicit mapping to the RKHS.

Lemma 1. Let \mathbf{Z} be the mixture of the samples of \mathbf{X} and \mathbf{Y} , that is, $\mathbf{Z} = \{\mathbf{z}_i\}_{i=1}^{N+M}$ where $\mathbf{z}_i = \mathbf{x}_i$ for $i \in \{1, \dots, N\}$ and $\mathbf{z}_i = \mathbf{y}_{i-N}$ for $i \in \{N+1, \dots, N+M\}$. Also, let \mathbf{K}_Z be the kernel matrix consisting of all normalized pairwise kernel evaluations of the samples in \mathbf{Z} , then $S(\pi_1 C_X + \pi_2 C_Y) = S(\mathbf{K}_Z)$ (Proof: See appendix A.3 in supplementary material).

Since the spectrum of \mathbf{K}_X and C_X have the same non-zero eigenvalues, and likewise \mathbf{K}_Y and C_Y , the divergence can be computed directly from samples in the input space as:

$$D_{JS}^{\kappa}(\mathbf{X}, \mathbf{Y}) = S(\mathbf{K}_Z) - (\pi_1 S(\mathbf{K}_X) + \pi_2 S(\mathbf{K}_Y)) \quad (10)$$

The expressive power of the selected kernel — or equivalently, the RKHS embedding — determines the capacity of the divergence to distinguish probability distributions.

3.2 Properties

The representation JS divergence inherits most of the properties of classical and quantum JS divergence. *Non-negativity:* $D_{JS}^{\omega}(\mathbf{X}, \mathbf{Y}) \geq 0$. *Positivity:* $D_{JS}^{\omega}(\mathbf{X}, \mathbf{Y}) = 0$ if and only if $\mathbf{X} = \mathbf{Y}$. *Symmetry:* $D_{JS}^{\omega}(\mathbf{X}, \mathbf{Y}) = D_{JS}^{\omega}(\mathbf{Y}, \mathbf{X})$. *Boundedness:* $D_{JS}^{\omega}(\mathbf{X}, \mathbf{Y}) \leq \log \frac{N+M}{\sqrt{NM}}$. Also, $D_{JS}^{\omega}(\mathbf{X}, \mathbf{Y})^{\frac{1}{2}}$ is a metric on the cone of uncentered covariance matrices in any dimension [43].

Theorem 2. Let $\mathbf{Z} = \{\mathbf{z}_i\}_{i=1}^{N+M}$ be the mixture of the samples of \mathbf{X} and \mathbf{Y} and let \mathbf{L} be a one-hot vector indicating the distribution (label) of each point $\mathbf{l}_i = [1, 0]$ for $i \in \{1, \dots, N\}$ and $\mathbf{l}_i = [0, 1]$ for $i \in \{N+1, \dots, N+M\}$. Then, the representation Jensen-Shannon divergence corresponds to the matrix-based mutual information ([33]) between the mixture of the samples and the labels.

$$D_{JS}^\kappa(\mathbf{X}, \mathbf{Y}) = I^\kappa(\mathbf{Z}; \mathbf{L}) = S(\mathbf{K}_Z) + S(\mathbf{K}_L) - S\left(\frac{\mathbf{K}_Z \odot \mathbf{K}_L}{\text{Tr}(\mathbf{K}_Z \odot \mathbf{K}_L)}\right), \quad (11)$$

Proof: See appendix A.2 in supplementary material

(11) corresponds to the kernel-based Jensen-Rényi divergence proposed in [32] in the limit when $\alpha = 1$.

3.2.1 Computational Complexity

To calculate (9) and (10) it is necessary to extract the eigenvalues of positive semidefinite matrices. The eigendecomposition of covariance matrices has $\mathcal{O}(D^3)$ time complexity, where D is the dimensionality of the RKHS which is independent of the sample size. In contrast, the eigendecomposition for kernel matrices has $\mathcal{O}(N^3)$ time complexity. For a large N we use covariance matrices.

4 Variational Estimation of JS-divergence

We can use the lower bound in (7) to derive a variational method for estimating JS divergence given only samples from \mathbb{P} and \mathbb{Q} . Accordingly,

$$D_{JS}(\mathbb{P}, \mathbb{Q}) = \sup_{\phi \in \Phi} D_{JS}^\phi(C_{\mathbb{P}}, C_{\mathbb{Q}}), \quad (12)$$

where Φ is the class of functions $\phi : \mathcal{X} \rightarrow \mathcal{H}$ satisfying the assumptions of Theorem 1. Given a finite set of samples, we choose Φ to be the family of functions $\phi_\omega \circ f_\omega : \mathcal{X} \rightarrow \mathcal{H}_D$ parameterized by a Deep Fourier Features Network (DFFN) with parameters $\omega \in \Omega$. A DFNN is a deep neural network f_ω with a Fourier Feature mapping ϕ_ω in the last layer, that is, $\phi_\omega \circ f_\omega = \phi_\omega(f_\omega(x))$ for which we can also adjust the parameters of the last layer.

Definition 2. (*JS divergence neural estimator*). Let $\Phi = \{\phi_\omega \circ f_\omega\}_{\omega \in \Omega}$ be the set of functions parameterized by a DFFN. We define the representation JS divergence estimator as:

$$\widehat{D}_{JS}(\mathbb{P}, \mathbb{Q}) = \sup_{\omega \in \Omega} D_{JS}^\omega(\mathbf{X}, \mathbf{Y}). \quad (13)$$

This technique is related to deep kernel learning, where a kernel is computed on top of a deep neural network to model distributions with complex structures. The idea is to leverage the expressive power of deep networks and combine it with the capacity of kernels to embed distributions in a reproducing kernel Hilbert space [44–46].

Additionally, we propose an alternative estimator of JS divergence by leveraging the scalability properties of the covariance matrices. Given k batches $\{\mathbf{X}_i\}_{i=1}^k$ coming from the same distribution \mathbb{P} , the total covariance of the whole dataset corresponds to the average of the covariance matrices of all batches, that is $\mathbf{C}_X = \frac{1}{k} \sum_{i=1}^k \mathbf{C}_{X_i}$. However, during optimization, the representation changes and thus the mapped data distributions. Therefore, we propose using Exponential Moving Averages of the covariances to keep information from the most recent batches and smooth out the JS divergence estimation (see algorithm 3 in appendix A.4).

5 Experiments

5.1 Neural JS divergence estimation

First, we evaluate the performance of our neural estimator of JS divergence in a tractable toy experiment. Here, $\mathbb{P} \sim p(x; l_p, s_p)$ and $\mathbb{Q} \sim p(x; l_q, s_q)$ are two Cauchy distributions with location parameters l_p and l_q and scale parameters $s_p = s_q = 1$. We vary the location parameter of \mathbb{Q} over time to achieve a desired divergence. We use a closed form of the JS divergence between Cauchy distributions derived in [47] to determine the location parameter (See appendix A.4 in supplementary

material for more details). Then, we apply algorithm 1 drawing $N = 512$ samples from both distributions at every epoch. We compare the estimates of the representation JS divergence against two variational lower bounds of JS divergence: \mathcal{F} -distance [23] and the NWJ estimator [48] used to train f-GANs [24]. Fig. 1 shows that the \mathcal{F} -distance exhibits high bias for small divergence values and high variance. NWJ correctly estimates small divergence values with low variance, but the estimates degrade when the divergence is high. In contrast to the compared methods, the representation JS divergence accurately estimates divergence at both small and high divergence values with a moderate variance. Additionally, by using EMA on the covariance matrices the estimation variance decreases yielding a smoother estimation. These results show empirically that the proposed lower bound is tight in small dimensions.

5.2 Generative Adversarial Networks

Generative Adversarial Networks (GANs) are a popular family of algorithms to perform image generation achieving state-of-the-art results [49, 50]. GANs are composed of two main components: a *generator* and a *discriminator*. The generator $G : \mathcal{Z} \rightarrow \mathcal{X}$ is trained to produce samples that match (resemble) a target distribution and the *discriminator* $D : \mathcal{X} \rightarrow [0, 1]$ is trained to distinguish between real and generated data. The optimization is commonly formulated as a minmax problem $\min_{G \in \mathcal{G}} \max_{D \in \mathcal{D}} V(G, D)$, where $V(G, D)$ is a learning function that measures the dissimilarity between the generated and the real data [51]. Clearly, divergences can be used to train GANs. The vanilla GAN algorithm [52] approximately minimizes the Jensen-Shannon divergence by using a lower bound based on the classification outputs of the discriminator as $\frac{1}{2}\mathbb{E}_{\mathbb{P}}[\log(D(x))] + \frac{1}{2}\mathbb{E}_{\mathbb{Q}}[\log(1 - D(x))] + \log(2)$. Similarly, Wasserstein GANs [25] and MMD GANs [53] have been proposed to minimize the distance between the generated and real distributions.

GANs usually suffer from mode collapse. The generated samples lack diversity and fail to cover the multiple modes (classes) of real data [30] yielding a lower entropy distribution with less heterogeneity than the real data [54]. This issue is usually attributed to using a classifier to measure the divergence since the generator can learn to create a few realistic samples to fool the discriminator and trivially minimize the loss. Besides, since the discriminator handles each example independently, there is a lack of coordination between the gradients, and consequently, the generator is not penalized by

Algorithm 1 JS divergence estimation

Input: $\mathbf{X} \sim \mathbb{P}, \mathbf{Y} \sim \mathbb{Q}, \eta$
1: $\omega \leftarrow$ Initialize network parameters parameters.
2: **for** $T = 1 : \text{Number of epochs}$ **do**
3: $\Phi_X \leftarrow \phi_\omega \circ f_\omega(\mathbf{X})$
4: $\Phi_Y \leftarrow \phi_\omega \circ f_\omega(\mathbf{Y})$
5: $\mathbf{C}_X \leftarrow \frac{1}{N} \Phi_X^T \Phi_X$
6: $\mathbf{C}_Y \leftarrow \frac{1}{M} \Phi_Y^T \Phi_Y$
7: $D_{JS}^\omega(\mathbf{X}, \mathbf{Y}) = S(\pi_1 \mathbf{C}_X + \pi_2 \mathbf{C}_Y) - (\pi_1 S(\mathbf{C}_X) + \pi_2 S(\mathbf{C}_Y))$ ▷ as in (9)
8: $\omega \leftarrow \omega + \eta \nabla_{\text{Adam}} D_{JS}^\omega(\mathbf{X}, \mathbf{Y})$ ▷ Maximize the divergence
9: **end for**
Output: $\widehat{D}_{JS}(\mathbb{P}, \mathbb{Q}) = D_{JS}^\omega(\mathbf{X}, \mathbf{Y})$

Algorithm 2 Representation JS divergence GAN

Input: $\mathbf{X}_P = \{\mathbf{X}_i\}_{i=1}^k \sim \mathbb{P}$
1: $\theta, \omega \leftarrow$ Initialize network parameters parameters.
2: **for** $T = 1 : \text{Number of epochs}$ **do**
3: **for** $i = 1 : k$ **do**
4: $\mathbf{Y}_i^\theta = g_\theta(\mathbf{z})$ ▷ Generated batch from random noise \mathbf{z}
5: $\omega \leftarrow \omega + \eta_d \nabla_{\text{Adam}} D_{JS}^\omega(\mathbf{X}_i, \mathbf{Y}_i^\theta)$ ▷ Maximize the divergence
6: $\theta \leftarrow \theta - \eta_g \nabla_{\text{Adam}} D_{JS}^\omega(\mathbf{X}_i, \mathbf{Y}_i^\theta)$ ▷ Minimize the divergence
7: **end for**
8: **end for**

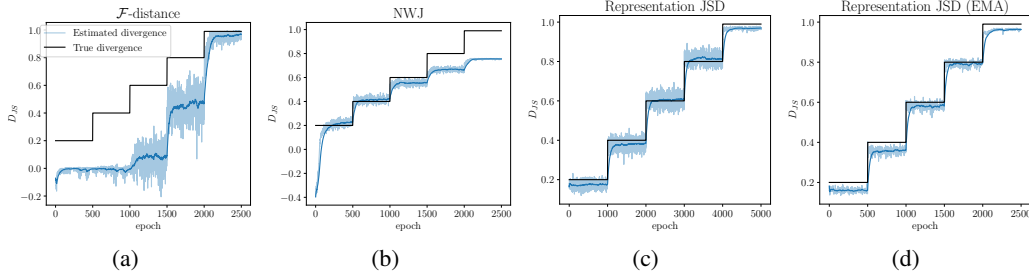


Figure 1: Jensen-Shannon Divergence estimation for two set of samples following Cauchy distributions ($N = 512$) (a) \mathcal{F} -distance [23] (b) NWJ estimator [48, 24] (c) Representation JS divergence (d) Representation JS divergence with exponentiated moving averages (EMA) of the covariances

producing similar samples [55]. Several approaches have been proposed to reduce mode collapse and encourage sample diversity. One common approach to prevent mode collapse is through entropy regularizers [27] where an estimator of mutual information is used as a proxy to regularize the entropy of the generated samples. Similarly, PresGANs [56] alleviate mode collapse by explicitly maximizing the entropy of the generative distribution.

Here, we propose to use the representation JS divergence to train GANs as follows:

$$\min_{G \in \mathcal{G}} \max_{\phi \in \Phi} D_{JS}^{\phi}(C_{\mathbb{P}}, C_{\mathbb{Q}}) \qquad \min_{\theta \in \Theta} \max_{\omega \in \Omega} D_{JS}^{\omega}(C_X, C_Y^{\theta}) \quad (14)$$

Compared to traditional GANs, we do not employ a discriminator in the strict sense, but we use a Deep Fourier Features Network (DFFN, see section 4). The DFFN plays the role of the discriminator, but instead of classifying real and fake samples, it learns a multidimensional representation in an RKHS that maximizes the divergence between the distributions. Subsequently, the generator adjusts itself to minimize the divergence induced by the DFFN. We follow a single-step alternating gradient method to optimize the divergence (See algorithm 2).

This formulation has several advantages. Our framework analyzes the covariance matrices of entire batches of real and generated data rather than individual samples. This leads to coordinated gradients that work to either increase or decrease the divergence between the distributions. By minimizing the representation JS divergence, our method ensures that the entropy of the generated samples is equivalent to that of the training distribution without auxiliary regularizers. This encourages diversity in the generated samples and helps prevent mode collapse by penalizing generated distributions that have lower entropy than the real distribution.

We apply the representation JS divergence to reduce mode collapse and enhance mode coverage when training a generative adversarial network. We assess our GAN formulation in two well-known mode-collapse experiments: 8 Gaussians dataset and Stacked MNIST.

5.2.1 Synthetic experiments

We applied the representation JS divergence to train a GAN in a synthetic experiment. The target distribution is a mixture of 8 Gaussian distributions arranged in a circle. Fig. 2 shows the real and generated samples by various learning functions used to train GANs. The generator and discriminator architectures are identical for all methods, except for the representation JS divergence that replaces the last layer of the discriminator by a Fourier Feature Layer (See implementation details in the supplementary material, appendix A.5.1). As expected, the standard (vanilla) GAN formulation fails to generate samples from all modes (Fig. 2(a)). The Hinge [57] and Wasserstein-GP GANs [58] successfully produce samples representing all 8 modes, yet, Fig. 2(b) and 2(c) demonstrate limited intra-class diversity, as the generated samples within each mode are closely clustered failing to cover the entire support of each Gaussian distribution. This leads to generated distributions with lower entropy (less diversity) compared to the real distribution. In contrast to the compared methods, the representation JS divergence shows both improved mode coverage and higher diversity of the generated samples. This is visually noticeable in Fig. 2(d) where the generated data capture the variability and diversity of every mode. This confirms our hypothesis that minimizing the representation JS divergence prevents mode-dropping and encourages sample diversity.

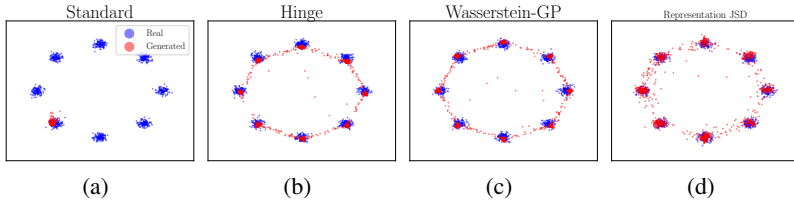


Figure 2: GANs with different loss functions to evaluate mode collapse in 8 Gaussians dataset. The representation JS divergence improves mode coverage and sample diversity.

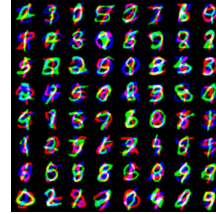


Figure 3: Generated samples using rep JSD.

5.2.2 Stacked MNIST

We conduct a quantitative evaluation to assess the efficacy of the representation JS divergence in reducing mode collapse on the stacked MNIST dataset. This dataset consists of 3 randomly sampled MNIST digits stacked along different color channels. This procedure results in 1000 possible classes (modes) corresponding to all possible combinations of the ten digits. We use the standard DCGAN generator architecture [59], and modify the discriminator architecture to include a Fourier Feature mapping (See implementation details in the supplementary material, appendix A.5.2). We compare our method against a considerable number of GAN algorithms using the same generator and following the same evaluation protocol. We utilize a pre-trained classifier on a set of 26,000 samples to quantify the number

Table 1: Number of captured modes and KL divergence between the real and generated distributions.

	Modes (Max 1000)	KL
DCGAN [59]	99.0	3.40
ALI [60]	16.0	5.40
Unrolled GAN [61]	48.7	4.32
VEEGAN [62]	150	2.95
WGAN-GP [58]	959.0	0.72
PresGAN [56]	999.6 ± 0.4	$0.11 \pm 7.0e-2$
PacGAN [63]	1000.0 ± 0	$0.06 \pm 1.0e-2$
GAN+MINE [27]	1000.0 ± 0	$0.05 \pm 6.9e-3$
GAN + rep JSD	1000.0 ± 0	$0.04 \pm 1.2e-3$

of distinct modes present within the generated samples. Additionally, we calculate the Kullback-Leibler (KL) divergence between the distribution of the modes of the generated samples and the real mode distribution. Finally, we averaged the results over five runs. Table 1 shows the results and the representation JS divergence captures all modes and steadily generates samples from all classes achieving the lowest KL-divergence compared to the baseline approaches. It is worth noting that our algorithm is essentially a standard GAN, that explicitly minimizes the JS divergence. Importantly, our approach does not require the incorporation of additional entropy regularizers or mode-collapse prevention mechanisms beyond the learning function itself.

5.3 Two sample testing

We evaluate the performance of the proposed divergence for two-sample testing on different datasets and compared it against different state-of-the-art methods. We perform the following tests: (a) JSD-FF: Two-sample test based on JS divergence using (9) optimizing the Fourier Features applied to the input data. (b) JSD-RFF: Two-sample test based on JS divergence using (9) using *Random Fourier Features*, optimizing just the length-scale of the associated Gaussian kernel. (c) JSD-D: Two-sample test based on JS divergence using a Deep Fourier Features Network (DFFN) as explained in section 4 (See implementation details in the supplementary material, appendix A.6). (d) JSD-K¹: Two-sample test based on the kernel representation JS divergence estimator (10) optimizing the length-scale of a Gaussian kernel. (e) MMD-O: Two-sample test based on MMD optimizing the length-scale of the Gaussian kernel as in [46]. (f) MMD-D: Two-sample test based on MMD with a deep kernel as in [46]. (g) C2ST-L: a classifier two-sample test [64] based on the output classification scores. (h) C2ST-S: a classifier two-sample test [65] based on the sign of the output classification scores.

We perform two-sample testing on one real-word and 2 synthetic datasets. The procedure is the following: for synthetic datasets, we create the sets $\mathbf{X}_{train} \in \mathbb{R}^{N \times d}$ and $\mathbf{Y}_{train} \in \mathbb{R}^{M \times d}$. Then, we learn the kernel/covariance/classifier for each of the methods on that training set. We then sample a testing set $\mathbf{X}_{test} \in \mathbb{R}^{N \times d}$ and $\mathbf{Y}_{test} \in \mathbb{R}^{M \times d}$ and perform a permutation test. We compute the

¹We did not perform this test for large size datasets due to computational restrictions

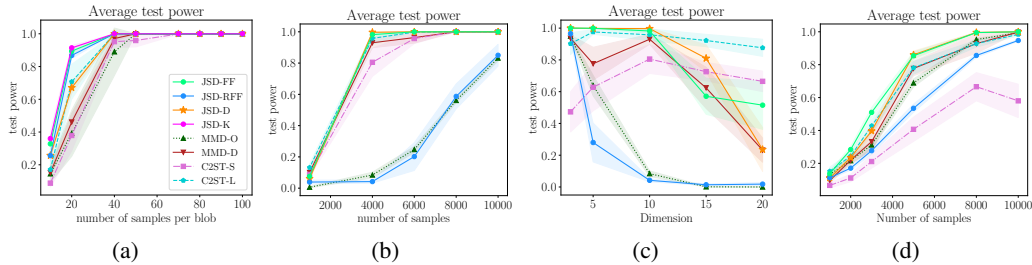


Figure 4: Average test power over 10 trials on the (a) Blobs dataset. (b) High dimensional Gaussian mixture, fixed $d = 10$. (c) High dimensional Gaussian mixture, fixed $N + M = 4000$ (d) Higgs dataset

statistic on the testing set and perform 100 permutations to generate the surrogate of the distribution of the measurement under the null hypothesis. Finally, we compute the rejection threshold, and if the statistic is greater than this threshold we reject the null hypothesis. This is done for 100 independent testing sets. Finally, we repeat the experiment ten times and compute the average test power. The number of Fourier Features and implementation details are discussed in the supplementary material (appendix A.6).

Blobs dataset [46]: In this dataset $\mathbf{X} \sim \mathbb{P}_X$ and $\mathbf{Y} \sim \mathbb{P}_Y$, where \mathbb{P}_X and \mathbb{P}_Y are mixtures of nine Gaussians with the same modes. Each mode of \mathbb{P}_X is an isotropic Gaussian, yet, the modes of \mathbb{P}_Y have different covariance. Here, we perform two sample testing for different number of samples per blob ($N = 9 \times$ samples per blob). Fig 4(a) shows the results and we can clearly see that JSD-FF, JSD-D and JSD outperform all state-of-the-art methods. We can evidence that even for a small number of samples the representation JSD-based methods exhibit high test power.

High-Dimensional Gaussian Mixtures [46]: We assess the performance of the representation JS divergence at high dimensions, on a bimodal multidimensional Gaussian dataset. In this dataset, \mathbb{P}_X and \mathbb{P}_Y have the same modes, and their covariances only differ on a single dimension. See [46] for details. We tested both changing the number of samples while keeping the dimension constant ($d = 10$) and maintaining the number of samples ($N = 4000$) while modifying the dimensionality. Figs. 4(b) and 4(c) display the results, where JSD-D and JSD-FF are the winners in most settings, although C2ST-L performs better at higher dimensions in this dataset.

Higgs dataset [66] : Following [46] we perform two-sample testing on the Higgs dataset ($d = 4$). We test the null hypothesis as we increase the number of samples and Fig. 4(d) shows the results. Once again, JSD-D and JSD-FF outperformed the baselines in almost all scenarios.

6 Conclusions

Our study presents a compelling divergence termed the representation Jensen-Shannon divergence, and a novel non-parametric estimator based on Fourier features. Notably, this estimator demonstrates scalability, differentiability, making it suitable for diverse machine-learning problems. We demonstrated that the representation Jensen-Shannon divergence provides a lower bound on the true Jensen-Shannon divergence, leading to a variational estimator of high precision compared to related approaches; although the bias and consistency of the estimators require further research. We leveraged this novel divergence to train generative networks, and the empirical results show that the representation Jensen-Shannon divergence effectively mitigates mode collapse, yielding generative models that produce more accurate and diverse results. Furthermore, when applied to two-sample testing, the representation Jensen-Shannon divergence surpassed other state-of-the-art techniques, demonstrating superior performance and reliability in discriminating between distributions. These findings highlight the significant practical implications of our divergence measure.

References

- [1] Yuhong Yang and Andrew Barron. Information-theoretic determination of minimax rates of convergence. *Annals of Statistics*, pages 1564–1599, 1999.
- [2] Bharath K Sriperumbudur, Kenji Fukumizu, Arthur Gretton, Bernhard Schölkopf, and Gert RG Lanckriet. On the empirical estimation of integral probability metrics. 2012.
- [3] Akshay Krishnamurthy, Kirthevasan Kandasamy, Barnabas Poczos, and Larry Wasserman. Nonparametric estimation of renyi divergence and friends. In *International Conference on Machine Learning*, pages 919–927. PMLR, 2014.
- [4] Kevin Moon and Alfred Hero. Multivariate f-divergence estimation with confidence. *Advances in neural information processing systems*, 27, 2014.
- [5] Shashank Singh and Barnabás Póczos. Generalized exponential concentration inequality for rényi divergence estimation. In *International Conference on Machine Learning*, pages 333–341. PMLR, 2014.
- [6] Yingzhen Li and Richard E Turner. Rényi divergence variational inference. *Advances in neural information processing systems*, 29, 2016.
- [7] Morteza Noshad, Kevin R Moon, Salimeh Yasaei Sekeh, and Alfred O Hero. Direct estimation of information divergence using nearest neighbor ratios. In *2017 IEEE International Symposium on Information Theory (ISIT)*, pages 903–907. IEEE, 2017.
- [8] Kevin R Moon, Kumar Sricharan, Kristjan Greenewald, and Alfred O Hero III. Ensemble estimation of information divergence. *Entropy*, 20(8):560, 2018.
- [9] Yuheng Bu, Shaofeng Zou, Yingbin Liang, and Venugopal V Veeravalli. Estimation of kl divergence: Optimal minimax rate. *IEEE Transactions on Information Theory*, 64(4):2648–2674, 2018.
- [10] Thomas B Berrett and Richard J Samworth. Efficient two-sample functional estimation and the super-oracle phenomenon. *arXiv preprint arXiv:1904.09347*, 2019.
- [11] Tengyuan Liang. Estimating certain integral probability metric (ipm) is as hard as estimating under the ipm. *arXiv preprint arXiv:1911.00730*, 2019.
- [12] Yanjun Han, Jiantao Jiao, Tsachy Weissman, and Yihong Wu. Optimal rates of entropy estimation over lipschitz balls. 2020.
- [13] Sreejith Sreekumar and Ziv Goldfeld. Neural estimation of statistical divergences. *Journal of machine learning research*, 23(126), 2022.
- [14] Sandesh Ghimire, Aria Masoomi, and Jennifer Dy. Reliable estimation of kl divergence using a discriminator in reproducing kernel hilbert space. *Advances in Neural Information Processing Systems*, 34:10221–10233, 2021.
- [15] Alfred Müller. Integral probability metrics and their generating classes of functions. *Advances in applied probability*, 29(2):429–443, 1997.
- [16] James M Joyce. Kullback-leibler divergence. In *International encyclopedia of statistical science*, pages 720–722. Springer, 2011.
- [17] ML Menéndez, JA Pardo, L Pardo, and MC Pardo. The jensen-shannon divergence. *Journal of the Franklin Institute*, 334(2):307–318, 1997.
- [18] Erik Englesson and Hossein Azizpour. Generalized jensen-shannon divergence loss for learning with noisy labels. *Advances in Neural Information Processing Systems*, 34:30284–30297, 2021.
- [19] Arthur Gretton, Karsten M Borgwardt, Malte J Rasch, Bernhard Schölkopf, and Alexander Smola. A kernel two-sample test. *The Journal of Machine Learning Research*, 13(1):723–773, 2012.

- [20] Ruize Gao, Feng Liu, Jingfeng Zhang, Bo Han, Tongliang Liu, Gang Niu, and Masashi Sugiyama. Maximum mean discrepancy test is aware of adversarial attacks. In *International Conference on Machine Learning*, pages 3564–3575. PMLR, 2021.
- [21] Soheil Kolouri, Kimia Nadjahi, Umut Simsekli, Roland Badeau, and Gustavo Rohde. Generalized sliced wasserstein distances. *Advances in neural information processing systems*, 32, 2019.
- [22] Dongha Kim, Kunwoong Kim, Insung Kong, Ilsang Ohn, and Yongdai Kim. Learning fair representation with a parametric integral probability metric. In *International Conference on Machine Learning*, pages 11074–11101. PMLR, 2022.
- [23] Sanjeev Arora, Rong Ge, Yingyu Liang, Tengyu Ma, and Yi Zhang. Generalization and equilibrium in generative adversarial nets (gans). In *International Conference on Machine Learning*, pages 224–232. PMLR, 2017.
- [24] Sebastian Nowozin, Botond Cseke, and Ryota Tomioka. f-gan: Training generative neural samplers using variational divergence minimization. *Advances in neural information processing systems*, 29, 2016.
- [25] Martin Arjovsky, Soumith Chintala, and Léon Bottou. Wasserstein generative adversarial networks. In *International conference on machine learning*, pages 214–223. PMLR, 2017.
- [26] Pengchuan Zhang, Qiang Liu, Dengyong Zhou, Tao Xu, and Xiaodong He. On the discrimination-generalization tradeoff in gans. *arXiv preprint arXiv:1711.02771*, 2017.
- [27] Mohamed Ishmael Belghazi, Aristide Baratin, Sai Rajeshwar, Sherjil Ozair, Yoshua Bengio, Aaron Courville, and Devon Hjelm. Mutual information neural estimation. In *International conference on machine learning*, pages 531–540. PMLR, 2018.
- [28] Youssef Mroueh, Igor Melnyk, Pierre Dognin, Jarret Ross, and Tom Sercu. Improved mutual information estimation. In *Proceedings of the AAAI Conference on Artificial Intelligence*, volume 35, pages 9009–9017, 2021.
- [29] Takeru Miyato, Toshiki Kataoka, Masanori Koyama, and Yuichi Yoshida. Spectral normalization for generative adversarial networks. *arXiv preprint arXiv:1802.05957*, 2018.
- [30] Jinyoung Choi and Bohyung Han. Mcl-gan: Generative adversarial networks with multiple specialized discriminators. *Advances in Neural Information Processing Systems*, 35:29597–29609, 2022.
- [31] Francis Bach. Information theory with kernel methods. *IEEE Transactions on Information Theory*, 2022.
- [32] Jhoan Keider Hoyos Osorio, Oscar Skean, Austin J Brockmeier, and Luis Gonzalo Sanchez Giraldo. The representation jensen-rényi divergence. In *ICASSP 2022-2022 IEEE International Conference on Acoustics, Speech and Signal Processing (ICASSP)*, pages 4313–4317. IEEE, 2022.
- [33] Luis Gonzalo Sanchez Giraldo, Murali Rao, and Jose C Principe. Measures of entropy from data using infinitely divisible kernels. *IEEE Transactions on Information Theory*, 61(1):535–548, 2014.
- [34] Jop Briët and Peter Harremoës. Properties of classical and quantum jensen-shannon divergence. *Physical review A*, 79(5):052311, 2009.
- [35] Suvrit Sra. Metrics induced by jensen-shannon and related divergences on positive definite matrices. *Linear Algebra and its Applications*, 616:125–138, 2021.
- [36] Ivan B Djordjevic. *Quantum Information Processing, Quantum Computing, and Quantum Error Correction: An Engineering Approach*. Academic Press, 2021.
- [37] Krikamol Muandet, Kenji Fukumizu, Bharath Sriperumbudur, Bernhard Schölkopf, et al. Kernel mean embedding of distributions: A review and beyond. *Foundations and Trends® in Machine Learning*, 10(1-2):1–141, 2017.

- [38] Martin Müller-Lennert, Frédéric Dupuis, Oleg Szehr, Serge Fehr, and Marco Tomamichel. On quantum rényi entropies: A new generalization and some properties. *Journal of Mathematical Physics*, 54(12):122203, 2013.
- [39] Shujian Yu, Luis Gonzalo Sanchez Giraldo, Robert Jenssen, and Jose C Principe. Multivariate extension of matrix-based rényi’s α -order entropy functional. *IEEE transactions on pattern analysis and machine intelligence*, 42(11):2960–2966, 2019.
- [40] Shujian Yu, Francesco Alesiani, Xi Yu, Robert Jenssen, and Jose Principe. Measuring dependence with matrix-based entropy functional. In *Proceedings of the AAAI Conference on Artificial Intelligence*, volume 35, pages 10781–10789, 2021.
- [41] John Von Neumann. *Mathematical foundations of quantum mechanics: New edition*, volume 53. Princeton university press, 2018.
- [42] Ali Rahimi and Benjamin Recht. Random features for large-scale kernel machines. *Advances in neural information processing systems*, 20, 2007.
- [43] Dániel Virosztek. The metric property of the quantum jensen-shannon divergence. *Advances in Mathematics*, 380:107595, 2021.
- [44] Andrew Gordon Wilson, Zhiting Hu, Ruslan Salakhutdinov, and Eric P Xing. Deep kernel learning. In *Artificial intelligence and statistics*, pages 370–378. PMLR, 2016.
- [45] Li Wenliang, Danica J Sutherland, Heiko Strathmann, and Arthur Gretton. Learning deep kernels for exponential family densities. In *International Conference on Machine Learning*, pages 6737–6746. PMLR, 2019.
- [46] Feng Liu, Wenkai Xu, Jie Lu, Guangquan Zhang, Arthur Gretton, and Danica J Sutherland. Learning deep kernels for non-parametric two-sample tests. In *International conference on machine learning*, pages 6316–6326. PMLR, 2020.
- [47] Frank Nielsen and Kazuki Okamura. On f-divergences between cauchy distributions. *IEEE Transactions on Information Theory*, 2022.
- [48] XuanLong Nguyen, Martin J Wainwright, and Michael I Jordan. Estimating divergence functionals and the likelihood ratio by convex risk minimization. *IEEE Transactions on Information Theory*, 56(11):5847–5861, 2010.
- [49] Tero Karras, Miika Aittala, Samuli Laine, Erik Härkönen, Janne Hellsten, Jaakko Lehtinen, and Timo Aila. Alias-free generative adversarial networks. In *Proc. NeurIPS*, 2021.
- [50] Axel Sauer, Katja Schwarz, and Andreas Geiger. Stylegan-xl: Scaling stylegan to large diverse datasets. In *ACM SIGGRAPH 2022 conference proceedings*, pages 1–10, 2022.
- [51] Farzan Farnia and Asuman Ozdaglar. Gans may have no nash equilibria. *arXiv preprint arXiv:2002.09124*, 2020.
- [52] Ian Goodfellow, Jean Pouget-Abadie, Mehdi Mirza, Bing Xu, David Warde-Farley, Sherjil Ozair, Aaron Courville, and Yoshua Bengio. Generative adversarial networks. *Communications of the ACM*, 63(11):139–144, 2020.
- [53] Chun-Liang Li, Wei-Cheng Chang, Yu Cheng, Yiming Yang, and Barnabás Póczos. Mmd gan: Towards deeper understanding of moment matching network. *Advances in neural information processing systems*, 30, 2017.
- [54] Tong Che, Yanran Li, Athul Paul Jacob, Yoshua Bengio, and Wenjie Li. Mode regularized generative adversarial networks. *arXiv preprint arXiv:1612.02136*, 2016.
- [55] Tim Salimans, Ian Goodfellow, Wojciech Zaremba, Vicki Cheung, Alec Radford, and Xi Chen. Improved techniques for training gans. *Advances in neural information processing systems*, 29, 2016.
- [56] Adji B Dieng, Francisco JR Ruiz, David M Blei, and Michalis K Titsias. Prescribed generative adversarial networks. *arXiv preprint arXiv:1910.04302*, 2019.

- [57] Jae Hyun Lim and Jong Chul Ye. Geometric gan. *arXiv preprint arXiv:1705.02894*, 2017.
- [58] Ishaan Gulrajani, Faruk Ahmed, Martin Arjovsky, Vincent Dumoulin, and Aaron C Courville. Improved training of wasserstein gans. *Advances in neural information processing systems*, 30, 2017.
- [59] Alec Radford, Luke Metz, and Soumith Chintala. Unsupervised representation learning with deep convolutional generative adversarial networks. *arXiv preprint arXiv:1511.06434*, 2015.
- [60] Vincent Dumoulin, Ishmael Belghazi, Ben Poole, Olivier Mastropietro, Alex Lamb, Martin Arjovsky, and Aaron Courville. Adversarially learned inference. *arXiv preprint arXiv:1606.00704*, 2016.
- [61] Luke Metz, Ben Poole, David Pfau, and Jascha Sohl-Dickstein. Unrolled generative adversarial networks. *arXiv preprint arXiv:1611.02163*, 2016.
- [62] Akash Srivastava, Lazar Valkov, Chris Russell, Michael U Gutmann, and Charles Sutton. Veegan: Reducing mode collapse in gans using implicit variational learning. *Advances in neural information processing systems*, 30, 2017.
- [63] Zinan Lin, Ashish Khetan, Giulia Fanti, and Sewoong Oh. Pacgan: The power of two samples in generative adversarial networks. *Advances in neural information processing systems*, 31, 2018.
- [64] Xiuyuan Cheng and Alexander Cloninger. Classification logit two-sample testing by neural networks for differentiating near manifold densities. *IEEE Transactions on Information Theory*, 68(10):6631–6662, 2022.
- [65] David Lopez-Paz and Maxime Oquab. Revisiting classifier two-sample tests. *arXiv preprint arXiv:1610.06545*, 2016.
- [66] Pierre Baldi, Peter Sadowski, and Daniel Whiteson. Searching for exotic particles in high-energy physics with deep learning. *Nature communications*, 5(1):4308, 2014.

A Appendix

Next, we present the proofs of the theorems and properties described in the paper. Additionally, we include implementation details for all the experiments reported. All the codes to reproduce the results in the paper can be found in the following Github repository: <https://github.com/uk-cliplab/representationJSD>.

A.1 Proof Theorem 1

Proof. For (7) we have the following

$$\begin{aligned}
D_{JS}(C_{\mathbb{P}}, C_{\mathbb{Q}}) &= \frac{1}{2}D_{KL}(C_{\mathbb{P}}, C_{\mathbb{M}}) + \frac{1}{2}D_{KL}(C_{\mathbb{Q}}, C_{\mathbb{M}}) \\
&= \frac{1}{2}D_{KL}\left(\int_{\mathcal{X}} \phi(x) \otimes \phi(x) d\mathbb{P}(x) \mid \int_{\mathcal{X}} \phi(x) \otimes \phi(x) d\mathbb{M}(x)\right) + \\
&\quad + \frac{1}{2}D_{KL}\left(\int_{\mathcal{X}} \phi(x) \otimes \phi(x) d\mathbb{Q}(x) \mid \int_{\mathcal{X}} \phi(x) \otimes \phi(x) d\mathbb{M}(x)\right) \\
&= \frac{1}{2}D_{KL}\left(\int_{\mathcal{X}} \phi(x) \otimes \phi(x) d\mathbb{P}(x) \mid \int_{\mathcal{X}} \frac{d\mathbb{M}}{d\mathbb{P}}(x) \phi(x) \otimes \phi(x) d\mathbb{P}(x)\right) + \\
&\quad + \frac{1}{2}D_{KL}\left(\int_{\mathcal{X}} \phi(x) \otimes \phi(x) d\mathbb{Q}(x) \mid \int_{\mathcal{X}} \frac{d\mathbb{M}}{d\mathbb{Q}}(x) \phi(x) \otimes \phi(x) d\mathbb{P}(x)\right).
\end{aligned}$$

Since D_{KL} is jointly convex, then

$$\begin{aligned}
D_{JS}(C_{\mathbb{P}}, C_{\mathbb{Q}}) &\leq \frac{1}{2} \int_{\mathcal{X}} D_{KL}\left(\phi(x) \otimes \phi(x) \mid \frac{d\mathbb{M}}{d\mathbb{P}}(x) \phi(x) \otimes \phi(x)\right) d\mathbb{P}(x) + \\
&\quad + \frac{1}{2} \int_{\mathcal{X}} D_{KL}\left(\phi(x) \otimes \phi(x) \mid \frac{d\mathbb{M}}{d\mathbb{Q}}(x) \phi(x) \otimes \phi(x)\right) d\mathbb{Q}(x).
\end{aligned}$$

Notice that $\phi(x) \otimes \phi(x)$ is a rank-1 covariance operator with one eigenvalue equal $\|\phi(x)\|^2 = 1$ and one eigen vector $\phi(x)$, therefore, it can be simplified as:

$$\begin{aligned}
D_{JS}(C_{\mathbb{P}}, C_{\mathbb{Q}}) &\leq \frac{1}{2} \int_{\mathcal{X}} D_{KL}\left(1 \mid \frac{d\mathbb{M}}{d\mathbb{P}}(x)\right) d\mathbb{P}(x) + \frac{1}{2} \int_{\mathcal{X}} D_{KL}\left(1 \mid \frac{d\mathbb{M}}{d\mathbb{Q}}(x)\right) d\mathbb{Q}(x) \\
&= \frac{1}{2} \int_{\mathcal{X}} D_{KL}\left(1 \mid \frac{d\mathbb{M}}{d\mathbb{P}}(x)\right) d\mathbb{P}(x) + \frac{1}{2} \int_{\mathcal{X}} D_{KL}\left(1 \mid \frac{d\mathbb{M}}{d\mathbb{Q}}(x)\right) d\mathbb{Q}(x) \\
&= \frac{1}{2} \int_{\mathcal{X}} -\log\left(\frac{d\mathbb{M}}{d\mathbb{P}}(x)\right) d\mathbb{P}(x) + \frac{1}{2} \int_{\mathcal{X}} -\log\left(\frac{d\mathbb{M}}{d\mathbb{Q}}(x)\right) d\mathbb{Q}(x) \\
&= \frac{1}{2}D_{KL}(\mathbb{P}, \mathbb{M}) + \frac{1}{2}D_{KL}(\mathbb{Q}, \mathbb{M}) = D_{JS}(\mathbb{P}, \mathbb{Q})
\end{aligned}$$

For (8), we use (Proposition 4.e) in [31]. We have that

$$D_{KL}(C_{\mathbb{P}} \mid C_{\mathbb{Q}}) \geq \frac{1}{2} \|C_{\mathbb{P}} - C_{\mathbb{Q}}\|_*^2 \geq \frac{1}{2} \|C_{\mathbb{P}} - C_{\mathbb{Q}}\|_{\text{HS}}^2 \quad (15)$$

Since

$$\begin{aligned}
D_{JS}(C_{\mathbb{P}}, C_{\mathbb{Q}}) &= \frac{1}{2}D_{KL}(C_{\mathbb{P}}, C_{\mathbb{M}}) + \frac{1}{2}D_{KL}(C_{\mathbb{Q}}, C_{\mathbb{M}}) \\
&\geq \frac{1}{4} \left\| C_{\mathbb{P}} - \frac{1}{2}(C_{\mathbb{P}} + C_{\mathbb{Q}}) \right\|_*^2 + \frac{1}{4} \left\| C_{\mathbb{Q}} - \frac{1}{2}(C_{\mathbb{P}} + C_{\mathbb{Q}}) \right\|_*^2 \\
&\geq \frac{1}{4} \left\| \frac{1}{2}C_{\mathbb{P}} - \frac{1}{2}C_{\mathbb{Q}} \right\|_*^2 + \frac{1}{4} \left\| \frac{1}{2}C_{\mathbb{Q}} - \frac{1}{2}C_{\mathbb{P}} \right\|_*^2 = \frac{1}{8} \|C_{\mathbb{P}} - C_{\mathbb{Q}}\|_*^2
\end{aligned}$$

and thus, $D_{JS}(C_{\mathbb{P}}, C_{\mathbb{Q}}) \geq \frac{1}{8} \|C_{\mathbb{P}} - C_{\mathbb{Q}}\|_*^2 \geq \frac{1}{8} \|C_{\mathbb{P}} - C_{\mathbb{Q}}\|_{\text{HS}}^2$. \square

Now, let $\phi : \mathcal{X} \mapsto \mathcal{H}$ then, and $\{e_\alpha\}$ be an orthonormal basis in \mathcal{H} , we have that

$$\begin{aligned}
\text{Tr}(\phi(x) \otimes \phi(x)\phi(y) \otimes \phi(y)) &= \sum_{\alpha} \langle \phi(x) \otimes \phi(x)\phi(y) \otimes \phi(y)e_{\alpha}, e_{\alpha} \rangle \\
&= \sum_{\alpha} \langle \phi(x) \langle \phi(x), \phi(y) \otimes \phi(y)e_{\alpha} \rangle, e_{\alpha} \rangle \\
&= \sum_{\alpha} \langle \phi(x) \langle \phi(x), \phi(y) \langle \phi(y), e_{\alpha} \rangle \rangle, e_{\alpha} \rangle \\
&= \sum_{\alpha} \langle \phi(x) \langle \phi(x), \phi(y) \rangle \langle \phi(y), e_{\alpha} \rangle, e_{\alpha} \rangle \\
&= \sum_{\alpha} \langle \phi(x), e_{\alpha} \rangle \langle \phi(x), \phi(y) \rangle \langle \phi(y), e_{\alpha} \rangle \\
&= \langle \phi(x), \phi(y) \rangle \sum_{\alpha} \langle \phi(x), e_{\alpha} \rangle \langle \phi(y), e_{\alpha} \rangle = \langle \phi(x), \phi(y) \rangle \langle \phi(x), \phi(y) \rangle \\
&= \langle \phi(x), \phi(y) \rangle^2 = \kappa(x, y)^2
\end{aligned}$$

Note that for $T : \mathcal{H} \mapsto \mathcal{H}$, $\text{Tr}(T^*T) = \sum_{\alpha} \langle Te_{\alpha}, Te_{\alpha} \rangle = \|T\|_{\text{HS}}^2$. In particular, if we have that $T = \phi(x) \otimes \phi(x) - \phi(y) \otimes \phi(y)$,

$$\begin{aligned}
\|\phi(x) \otimes \phi(x) - \phi(y) \otimes \phi(y)\|_{\text{HS}}^2 &= \text{Tr}(\phi(x) \otimes \phi(x)\phi(x) \otimes \phi(x)) - 2 \text{Tr}(\phi(x) \otimes \phi(x)\phi(y) \otimes \phi(y)) \\
&\quad + \text{Tr}(\phi(y) \otimes \phi(y)\phi(y) \otimes \phi(y)) \\
&= \kappa^2(x, x) - 2\kappa^2(x, y) + \kappa^2(y, y)
\end{aligned}$$

Finally, note that

$$\begin{aligned}
\|C_{\mathbb{P}} - C_{\mathbb{Q}}\|_{\text{HS}}^2 &= \text{Tr}(\mathbb{E}_{\mathbb{P}}[\phi(x) \otimes \phi(x)]\mathbb{E}_{\mathbb{P}'}[\phi(x) \otimes \phi(x)]) - 2 \text{Tr}(\mathbb{E}_{\mathbb{P}}[\phi(x) \otimes \phi(x)]\mathbb{E}_{\mathbb{Q}}[\phi(y) \otimes \phi(y)]) \\
&\quad + \text{Tr}(\mathbb{E}_{\mathbb{Q}}[\phi(y) \otimes \phi(y)]\mathbb{E}_{\mathbb{Q}'}[\phi(y) \otimes \phi(y)]) \\
&= \text{Tr}(\mathbb{E}_{\mathbb{P}, \mathbb{P}'}[\phi(x) \otimes \phi(x)\phi(x') \otimes \phi(x')]) - 2 \text{Tr}(\mathbb{E}_{\mathbb{P}, \mathbb{Q}}[\phi(x) \otimes \phi(x)\phi(y) \otimes \phi(y)]) \\
&\quad + \text{Tr}(\mathbb{E}_{\mathbb{Q}, \mathbb{Q}'}[\phi(y) \otimes \phi(y)\phi(y') \otimes \phi(y')]) \\
&= \mathbb{E}_{\mathbb{P}, \mathbb{P}'}[\kappa^2(x, x')] - 2\mathbb{E}_{\mathbb{P}, \mathbb{Q}}[\kappa^2(x, y)] + \mathbb{E}_{\mathbb{Q}, \mathbb{Q}'}[\kappa^2(y, y')],
\end{aligned}$$

which corresponds to MMD with kernel $\kappa^2(\cdot, \cdot)$.

A.2 Proof Theorem 2

Proof. The matrix-based mutual information is defined as:

$$I^{\omega}(\mathbf{Z}; \mathbf{L}) = S(\mathbf{K}_{\mathbf{Z}}) + S(\mathbf{K}_{\mathbf{L}}) - S(\mathbf{K}_{\mathbf{z}}; \mathbf{K}_{\mathbf{L}}), \quad (16)$$

where $\mathbf{K}_{\mathbf{L}} = \mathbf{L}\mathbf{L}^{\top}$ and $S(\mathbf{K}_{\mathbf{z}}; \mathbf{K}_{\mathbf{L}})$ is the joint matrix-based entropy of the mixture and the labels. For simplicity let us assume $N = M$ (This can be easily generalized for $N \neq M$) and let \odot denote Hadamard product. Then, the joint entropy can be simplified as:

$$\begin{aligned}
S(\mathbf{K}_Z, \mathbf{K}_L) &= S(\mathbf{K}_Z \odot \mathbf{K}_L) \\
&= -\frac{1}{2} \sum_i \lambda_i(\mathbf{K}_X) \log \left[\frac{1}{2} \lambda_i(\mathbf{K}_X) \right] - \frac{1}{2} \sum_i \lambda_i(\mathbf{K}_Y) \log \left[\frac{1}{2} \lambda_i(\mathbf{K}_Y) \right] \\
&= -\frac{1}{2} \sum_i \lambda_i(\mathbf{K}_X) \log [\lambda_i(\mathbf{K}_X)] - \frac{1}{2} \sum_i \lambda_i(\mathbf{K}_X) \log \frac{1}{2} - \\
&\quad \frac{1}{2} \sum_i \lambda_i(\mathbf{K}_Y) \log [\lambda_i(\mathbf{K}_Y)] - \frac{1}{2} \sum_i \lambda_i(\mathbf{K}_Y) \log \frac{1}{2} \\
&= -\frac{1}{2} \sum_i \lambda_i(\mathbf{K}_X) \log [\lambda_i(\mathbf{K}_X)] - \frac{1}{2} \log \frac{1}{2} - \\
&\quad \frac{1}{2} \sum_i \lambda_i(\mathbf{K}_Y) \log [\lambda_i(\mathbf{K}_Y)] - \frac{1}{2} \log \frac{1}{2} \\
&= \frac{1}{2} S(\mathbf{K}_X) + \frac{1}{2} S(\mathbf{K}_Y) + \log(2).
\end{aligned}$$

Finally,

$$I^\kappa(\mathbf{Z}; \mathbf{L}) = S(\mathbf{K}_Z) - \frac{1}{2} (S(\mathbf{K}_X) + S(\mathbf{K}_Y)) = D_{JS}^\kappa(\mathbf{X}, \mathbf{Y}) \quad (17)$$

□

A.3 Proof of Lemma 1

Proof. Notice that the sum of covariance matrices in the RKHS corresponds to the concatenation of samples in the input space, that is:

$$\pi_1 \mathbf{C}_X + \pi_2 \mathbf{C}_Y = \frac{1}{N+M} \Phi_X^\top \Phi_X + \frac{1}{N+M} \Phi_Y^\top \Phi_Y \quad (18)$$

$$= \frac{1}{N+M} \begin{bmatrix} \Phi_X^\top & \Phi_Y^\top \end{bmatrix} \begin{bmatrix} \Phi_X \\ \Phi_Y \end{bmatrix} \quad (19)$$

$$= \frac{1}{N+M} \Phi_Z^\top \Phi_Z = \mathbf{C}_Z, \quad (20)$$

where $\Phi_Z = \begin{bmatrix} \Phi_X^\top & \Phi_Y^\top \end{bmatrix}^\top \in \mathbb{R}^{(N+M) \times D}$ contains the mappings of the mixture (concatenation) of the samples in the input space \mathbf{Z} . Since the spectrum of \mathbf{C}_Z and \mathbf{K}_Z have the same non-zero eigenvalues, $S(\pi_1 \mathbf{C}_X + \pi_2 \mathbf{C}_Y) = S(\mathbf{C}_Z) = S(\mathbf{K}_Z)$ □

A.4 Neural JS divergence estimation

Jensen-Shannon divergence between Cauchy distributions: The Jensen-Shannon for two Cauchy distributions $\mathbb{P} \sim p(x; l_p, s_p)$ and $\mathbb{Q} \sim p(x; l_q, s_q)$ can be estimated as [47]:

$$D_{JS}(\mathbb{P}, \mathbb{Q}) = \log \left(\frac{2\sqrt{(l_p - l_q)^2 + (s_p + s_q)^2}}{\sqrt{(l_p - l_q)^2 + (s_p + s_q)^2} + 2\sqrt{s_p s_q}} \right) \quad (21)$$

In this experiment we set $s_p = s_q = 1$, and $l_p = 0$. Then we calculate the value of l_q to achieve a specified divergence value in the set $\{0.2, 0.4, 0.6, 0.8, 0.99\}$.

Baselines: The \mathcal{F} -distance estimator [23] is a generalization of the standard loss used in GANs. Here, you train a classifier and estimate the JS divergence based on the classification scores as:

$$d_{\mathcal{F}}(\mathbb{P}, \mathbb{Q}) = \frac{1}{2} \mathbb{E}_{\mathbb{P}} [\log(D(x))] + \frac{1}{2} \mathbb{E}_{\mathbb{Q}} [\log(1 - D(x))] + \log(2), \quad (22)$$

The NWJ estimator is the one used to perform variational divergence minimization introduced in [24] to estimate JS divergence.

Implementation details and hyperparameters: Next, we show all the configurations that we used to perform the JS divergence estimation using the representation JS divergence. For this experiment, we use the covariance estimator by using Random Fourier Features (RFFs) to approximate a Gaussian kernel. We chose 50 RFFs and an initial kernel length scale $\sigma = 2$. We set the learning rate as $l_r = 0.001$ and we use the default β_1 and β_2 of the Adam optimizer. We did not use a deep neural network, but the Fourier Features layer by itself. We then applied algorithm 1 to learn ω and σ . We also implemented a version of the algorithm using exponential moving averages (EMA) of the covariance matrices. Specifically, we store information from past covariances and applied EMA to smooth out the estimation. Algorithm 3 shows a detailed explanation of this implementation.

Algorithm 3 JS divergence estimation EMA

Input: $\mathbf{X} \sim \mathbb{P}, \mathbf{Y} \sim \mathbb{Q}, \eta, \alpha$

- 1: $\omega \leftarrow$ Initialize network parameters parameters.
- 2: **for** $T = 1$: Number of epochs **do**
- 3: $\Phi_X; \Phi_Y$ ▷ Compute the mappings
- 4: $\mathbf{C}_X; \mathbf{C}_Y$ ▷ Compute the covariance matrices
- 5: **if** $T = 1$ **then**
- 6: $\widehat{\mathbf{C}}_X[T] = \mathbf{C}_X$
- 7: $\widehat{\mathbf{C}}_Y[T] = \mathbf{C}_Y$ ▷ Store previous covariance matrices
- 8: **else**
- 9: $\widehat{\mathbf{C}}_X[T] \leftarrow (1 - \alpha)\widehat{\mathbf{C}}_X[T - 1] + \alpha\mathbf{C}_X$
- 10: $\widehat{\mathbf{C}}_Y[T] \leftarrow (1 - \alpha)\widehat{\mathbf{C}}_Y[T - 1] + \alpha\mathbf{C}_Y$ ▷ Compute EMA covariance matrices
- 11: **end if**
- 12: $D_{JS}^\omega(\mathbf{X}, \mathbf{Y}) = S\left(\pi_1\widehat{\mathbf{C}}_X[T] + \pi_2\widehat{\mathbf{C}}_Y[T]\right) - \left(\pi_1S(\widehat{\mathbf{C}}_X[T]) + \pi_2S(\widehat{\mathbf{C}}_Y[T])\right)$
- 13: $\omega \leftarrow \omega + \eta\nabla_{\text{Adam}}D_{JS}^\omega(\mathbf{X}, \mathbf{Y})$ ▷ Maximize the divergence
- 14: **end for**

Output: $\widehat{D}_{JS}(\mathbb{P}, \mathbb{Q}) = D_{JS}^\omega(\mathbf{X}, \mathbf{Y})$

A.5 Generative Adversarial Networks

A.5.1 Mode Collapse experiments

To perform the mode collapse experiments, we used the code provided in https://github.com/ChristophReich1996/Mode_Collapse to compare GAN losses. To make a fair comparison, the generators of the compared losses are the same. The representation JS divergence does not rely on a discriminator or classifier, however, we used a Deep Fourier Features Network (DFFN) with a similar architecture to the discriminator that we used for the compared losses. Table 2 describes in detail the architectures employed.

For the representation JS divergence, we set the learning rate for the discriminator as $l_d = 1 \times 10^{-4}$ and the learning rate of the generator as $l_g = 5 \times 10^{-4}$. For Wasserstein-GP and Hinge losses, we used $l_d = l_g = 1 \times 10^{-4}$. For the standard GAN loss we used $l_d = 5 \times 10^{-4}$ and $l_r = 1 \times 10^{-4}$. We chose random uniform noise $z \sim \mathcal{U}^{32}[0, 1]$.

A.5.2 Stacked MNIST implementation details

Next, we describe the architecture and hyperparameters selection that we used to train a GAN in the stacked MNIST dataset, as well as some practical considerations. We used the standard DCGAN generator architecture [59] and slightly modified the discriminator architecture to incorporate a Fourier Feature Layer. Table 3 describes in detail the architecture employed. As you can see, we removed all batch norm layers in the discriminator and added two linear layers before the Fourier Feature mapping to reduce the high dimensionality of the last convolutional layer. We resized the images to $64 \times 64 \times 3$ to be compatible with the standard DCGAN architecture.

Table 2: Architectures mode collapse experiments

Generator	Discriminator	DFFN
Linear(32,256)	Linear(2,256)	Linear(2,256)
Leaky ReLU(0.01)	Leaky ReLU(0.01)	Leaky ReLU(0.01)
Linear(256,256)	Linear(256,256)	Linear(256,256)
Leaky ReLU(0.01)	Leaky ReLU(0.01)	Leaky ReLU(0.01)
Linear(256,256)	Linear(256,256)	Linear(256,256)
Leaky ReLU(0.01)	Leaky ReLU(0.01)	Leaky ReLU(0.01)
Linear(256,256)	Linear(256,256)	Linear(256,256)
tanH()	Leaky ReLU(0.01)	Leaky ReLU(0.01)
Linear(256,2)	Linear(256, 1)	Fourier Features Layer(256, 8)

Table 3: Architecture GAN on stacked MNIST. We use the following notation for the convolutional layers: ConvLayer(input channels, output channels, kernel size, stride, padding)

Generator	DFFN
ConvTranspose2d(100,512,4,1,0)	Conv2d(3, 64, 4, 2, 1)
Batchnorm()	LeakyReLU(0.2)
ReLU()	Conv2d(64, 128, 4, 2, 1)
ConvTranspose2d(512,256,4,2,1)	LeakyReLU(0.2)
Batchnorm()	Conv2d(128, 256, 4, 2, 1)
ReLU()	LeakyReLU(0.2)
ConvTranspose2d(256,128,4,2,1)	Conv2d(256, 512, 4, 2, 1)
Batchnorm()	LeakyReLU(0.2)
ReLU()	Flatten()
ConvTranspose2d(128,64 ,4,2,1)	Linear(8192, 512)
Batchnorm()	LeakyReLU(0.2)
ReLU()	Linear(512, 256)
ConvTranspose2d(64,3,4,2,1)	Fourier Features Layer (256, 4)
tanH()	

We draw z from a truncated Gaussian of 100 dimensions, with truncation parameter $\tau = 0.5$, where values that fall outside τ times the standard deviation are resampled to fall inside the range. This is known as the truncation trick.

We set the batch size as 64, and we train the GAN for 15 epochs. We set the discriminator’s learning rate as $l_d = 2.0 \times 10^{-5}$ whereas the generator’s as $l_g = 1.0 \times 10^{-4}$. We chose $\beta_1 = 0.5$ and $\beta_2 = 0.999$ as the hyperparameters of the Adam optimizer.

Here are some practical considerations to train a GAN with the representation JS divergence. First, the learning rates are crucial. If we use a high learning rate for the discriminator, it leads to a 0.99 divergence value, which the generator is not able to reduce. In contrast, if the discriminator’s learning rate is too small, then the divergence will remain close to 0 and the algorithm will not learn. So it is really important to choose the learning rates so that the divergence can grow quickly in the first steps but then the generator should be able to lower the divergence quickly too. Figure 5 shows the loss behavior during training with the selected learning rates. We also observed that a small number of Fourier Features (4 Fourier features, leading to 8 dimensions) lead to better results and make the algorithm easier and faster to train. We observed empirically that a large number of Fourier Features — although they could potentially capture richer information — makes the model prone to overfitting, yielding a high divergence regardless of what the generator does, the divergence stays high.

A.6 Two-sample testing

JSD-D test implementation details In this experiment, we try a slightly different implementation of the proposed covariance estimator using a deep Fourier Features network. We explore the idea of deep kernel learning by following a similar approach to [46], where a characteristic kernel $\kappa_\omega(x, y)$ is built as follows:

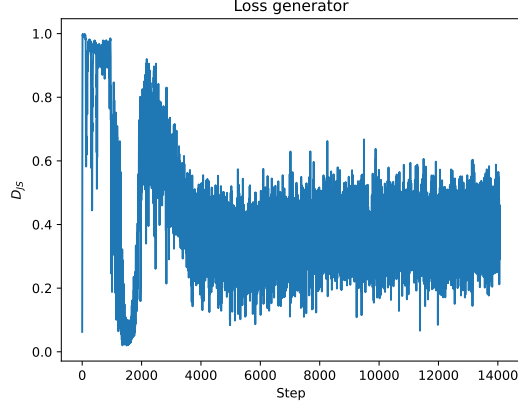


Figure 5: Loss GAN on the stacked MNIST dataset.

$$\kappa_\omega(x, y) = [(1 - \epsilon)\kappa_1(f_\omega(x), f_\omega(y)) + \epsilon]\kappa_2(x, y), \quad (23)$$

$$= (1 - \epsilon)\kappa_1(f_\omega(x), f_\omega(y))\kappa_2(x, y) + \epsilon\kappa_2(x, y) \quad (24)$$

where $f_\omega : \mathcal{X} \rightarrow \mathcal{F}$ is a deep network that extracts features from the data, allowing the kernel to have more flexibility to capture more accurately the structure of complicated distributions. $0 < \epsilon < 1$ and κ_1 and κ_2 are Gaussian kernels. Notice, that the kernel of the deep network features, κ_1 , is multiplied by another kernel κ_2 on the input space. This approach prevents the deep kernel from considering distant points in the input space as very similar.

In this work, we extend this idea to covariance operators and we propose a similar approach to learn deep covariance operators by learning an explicit mapping to the RKHS of a deep kernel. In first place, consider the product $\kappa_p(x, y) = \kappa_1(f_\omega(x), f_\omega(y))\kappa_2(x, y)$. Assuming $\kappa_\sigma = \kappa_1 = \kappa_2$ are Gaussian kernels with bandwidth σ , then $\kappa_p(x, y) = \kappa_\sigma(f_\omega(x) \oplus x, f_\omega(y) \oplus y)$, where \oplus stands for concatenation of the dimensions, that is, κ_p would be the kernel applied to the concatenation of the features from the deep network and the features in the input space. Afterward, we can use Fourier Features to learn an explicit mapping $\phi_\omega : \mathcal{X} \oplus \mathcal{F} \rightarrow \mathcal{H}_\phi$ to approximate a given shift-invariant kernel. Notice, that this approach is nothing but a linear layer with random weights $\omega \sim p(\omega)$ and sines and cosines as activation functions. Therefore $\kappa_p(x, y) \approx \langle \phi_\omega(f_\omega(x) \oplus x), \phi_\omega(f_\omega(y) \oplus y) \rangle_{\mathcal{H}_\phi}$. $\kappa_2(x, y)$ can be similarly approximated through a Fourier Feature mapping $\psi_\omega : \mathcal{X} \rightarrow \mathcal{H}_\psi$ applied directly on the samples in the input space, that is $\kappa_2(x, y) \approx \langle \psi_\omega(x), \psi_\omega(y) \rangle_{\mathcal{H}_\psi}$.

Finally, consider the whole kernel $\kappa_\omega(x, y) = (1 - \epsilon)\kappa_p(x, y) + \epsilon\kappa_2(x, y)$, which is the direct sum of two kernels with approximated explicit mappings ϕ_ω and ψ_ω respectively. By the properties of RKHS, it can be shown that:

$$\begin{aligned} \kappa_\omega(x, y) &= (1 - \epsilon)\kappa_p(x, y) + \epsilon\kappa_2(x, y) \\ &\approx \langle \varphi_\omega(x), \varphi_\omega(y) \rangle_{\mathcal{H}}, \end{aligned} \quad (25)$$

where $\varphi_\omega(x) = \left[(1 - \epsilon)^{\frac{1}{2}} \phi_\omega(x') \right] \oplus \left[\epsilon^{\frac{1}{2}} \psi_\omega(x) \right]$, $\mathcal{H} = \mathcal{H}_\psi \oplus \mathcal{H}_\phi$ and $x' = f_\omega(x) \oplus x$.

This procedure allows us to obtain an explicit mapping to the RKHS from a deep kernel that can be used to compute an explicit covariance operator. Consequently, this covariance operator can be optimized to maximize the JS divergence between the distributions. Note, that we can learn the parameters of the network f_ω as well as the Fourier Features ω and the kernel bandwidth σ .

Two-sample testing implementation details We run all baselines using the official implementation, that is MMD-O and MMD-D [46]², C2ST-S and C2ST-L [64]³. We follow all the configuration

²<https://github.com/fengliu90/DK-for-TST>

³https://github.com/xycheng/net_logit_test/tree/main

Table 4: Architecture of the Deep Fourier Features Network (DFFN) used in two sample testing. d is the input dimensionality, H is the number of hidden neurons and FF is the number of Fourier Features.

DFFN
Linear(d, H)
Softplus()
Linear(H, H)
Softplus()
Linear(H, H)
Softplus()
Linear(H, H)
Fourier Features Layer (H, FF)

and architecture proposed in [46]. To perform JSD-D, we used the same architecture as MMD-D, although, we add a Fourier Feature layer where MMD-D computes a kernel. Table 4 shows the details of the architecture used. The base network consists of five fully connected layers, and the number of neurons in hidden and output layers is set to 50 for Blob, $3 \times d$ for HDGM, and 20 for the Higgs dataset, where d is the dimension of the dataset. Also, the number of Fourier Features for all JSD-based tests is set to 50 for Blob, 15 for HDGM, and 15 for the Higgs dataset.

We use Adam optimizer to optimize 1) The kernel length scale σ in JSD-K and JSD-RFF 2) the Fourier Features ω and kernel length scale σ in JSD-FF and 3) the network parameters $\omega \in \Omega$, the Fourier Features ω and the kernel length scale σ in JSD-D. For the blobs dataset, we set the learning rate of JSD-FF, JSD-RFF and JSD-D as $l_r = 1 \times 10^{-3}$. For the HDGM, we set the learning rate for JSD-FF and JSD-RFF as $l_r = 5 \times 10^{-3}$, and the one for JSD-D as $l_r = 5 \times 10^{-2}$. In the Higgs dataset, we set all the learning rates as $l_r = 1 \times 10^{-2}$.

Figures 6 7,8,9 show the average test power and the standard deviation of each of the implemented test.

A.7 Limitations

Although the representation Jensen-Shannon divergence shows promising results, there are still some aspects that require further research. In particular, the bias and consistency of the estimators have not been studied. The analysis of the approximation and the empirical estimation errors is crucial to understanding the performance of the proposed approach. So far, the number of Fourier Features to build the reproducing kernel Hilbert space (RKHS) has been chosen arbitrarily. Empirically, we have found that choosing $D \ll N$ usually leads to better results, which could seem counter-intuitive with the kernel theory that usually induces a high-dimensional space. Also, using the kernel-based estimator for maximization purposes would require enforcing constraints on the scale of the data since this estimator can potentially exhibit rank-inconsistency of the matrices, that is $\max \text{Rank}(\mathbf{K}_Z) = N + M$, $\max \text{Rank}(\mathbf{K}_X) = N$ and $\max \text{Rank}(\mathbf{K}_Y) = M$. If the data scale is not kept fixed, trivial maximization of the divergence by just spreading all the samples far apart in the space, or equivalently for a Gaussian kernel by decreasing the length-scale σ can occur. For this reason, we employed the covariance-based estimator with a finite dimension (explicit feature space) in our experiments.

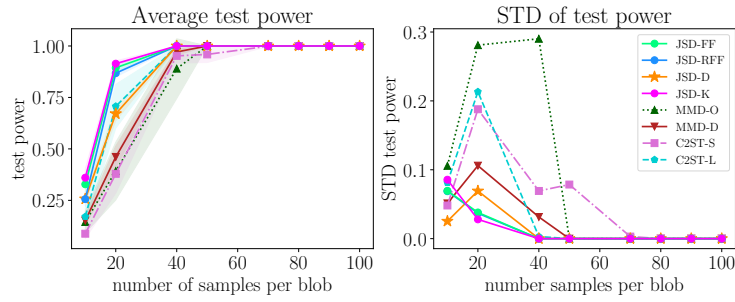


Figure 6: Power test for the blobs experiment.

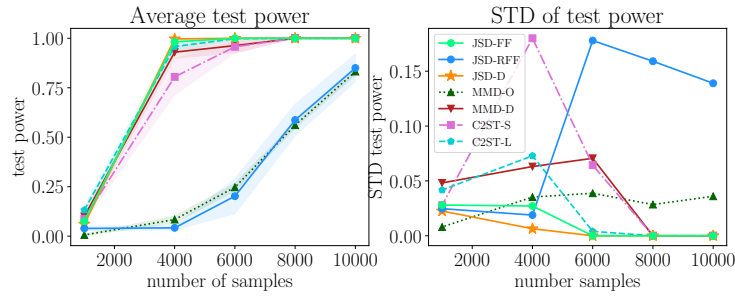


Figure 7: Power test for HDGM fixed N.

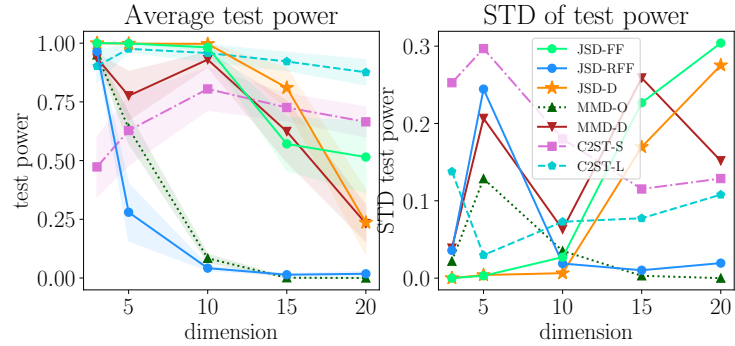


Figure 8: Power test for HDGM fixed d.

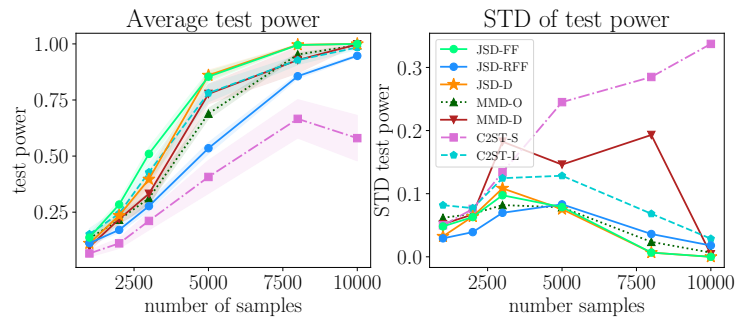


Figure 9: Power test for the Higgs dataset.